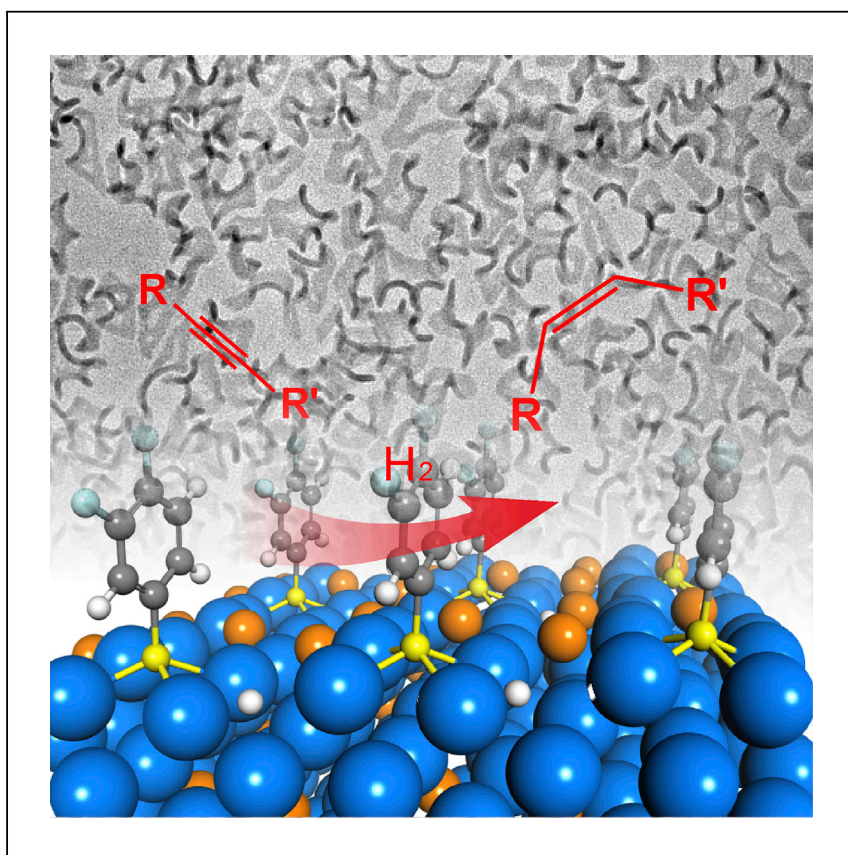


Article

Thiol Treatment Creates Selective Palladium Catalysts for Semihydrogenation of Internal Alkynes



Thiol treatment is demonstrated as a highly effective strategy for promoting the catalytic selectivity of Pd nanocatalysts in the hydrogenation of internal alkynes to alkenes.

Xiaojing Zhao, Lingyun Zhou,
Wuyong Zhang, ..., Binghui Wu,
Gang Fu, Nanfeng Zheng

gfu@xmu.edu.cn (G.F.)
nfzheng@xmu.edu.cn (N.Z.)

HIGHLIGHTS

Thiol-treated ultrathin Pd nanosheets are used as a model catalyst

The catalyst exhibits both high activity and selectivity in alkyne semihydrogenation

Both steric and electronic effects contribute to the enhanced selective hydrogenation

Practical Pd catalysts for semihydrogenation of internal alkynes are prepared



Article

Thiol Treatment Creates Selective Palladium Catalysts for Semihydrogenation of Internal Alkynes

Xiaojing Zhao,^{1,2} Lingyun Zhou,^{1,2} Wuyong Zhang,¹ Chengyi Hu,¹ Lei Dai,¹ Liting Ren,¹ Binghui Wu,¹ Gang Fu,^{1,*} and Nanfeng Zheng^{1,3,*}

SUMMARY

Surface and interfacial engineering of heterogeneous metal catalysts is effective and critical for optimizing selective hydrogenation for fine chemicals. By using thiol-treated ultrathin Pd nanosheets as a model catalyst, we demonstrate the development of stable, efficient, and selective Pd catalysts for semihydrogenation of internal alkynes. In the hydrogenation of 1-phenyl-1-propyne, the thiol-treated Pd nanosheets exhibited excellent catalytic selectivity (>97%) toward the semihydrogenation product (1-phenyl-1-propene). The catalyst was highly stable and showed no obvious decay in either activity or selectivity for over ten cycles. Systematic studies demonstrated that a unique Pd-sulfide/thiolate interface created by the thiol treatment was crucial to the semihydrogenation. The high catalytic selectivity and activity benefited from the combined steric and electronic effects that inhibited the deeper hydrogenation of C=C bonds. More importantly, this thiol treatment strategy is applicable to creating highly active and selective practical catalysts from commercial Pd/C catalysts for semihydrogenation of internal alkynes.

INTRODUCTION

Selective hydrogenation lies at the heart of industrial manufacture of fine chemicals, pharmaceuticals, nutraceuticals, and agrochemicals.^{1–4} To achieve a high yield of target product in an economical, energy-saving, and environmentally benign way, more and more attention has been paid to developing sustainable catalysts for selective hydrogenation.^{5–8} As for heterogeneous metal catalysts, the enhanced catalytic selectivity is mainly attributed to the electronic effects as a result of perturbation of the metal coordinative environment and/or steric effects induced by surface modifiers.^{9–13} Currently, two major approaches are used to tailor heterogeneous catalysts for selective hydrogenation: (1) the construction of multimetallic nanomaterials that provide ensemble control and electronic contributions for the adsorption of reactants and products and (2) the surface modification of metal nanoparticles for regulating the metal-organic interaction and thus improving the catalytic selectivity.^{14,15} Although the approaches have been applied for decades in academia and industry,^{16,17} the structure-activity relationship has not yet been well established because of the complexity of additives (often toxic), the diverse surfaces, and the mysterious interface structure.^{18–21}

In the fine chemical industry, selective hydrogenation of carbon-carbon triple bonds to carbon-carbon double bonds is a great challenge. The common industrial catalysts for alkyne hydrogenation are palladium-based catalysts.^{20,22–31} The surfaces

The Bigger Picture

The development of next-generation catalytic materials requires a methodological shift from trial-and-error to mechanism-directed design. It is highly desirable to build model catalyst systems with simplified structures to ensure maximized utilization of both state-of-the-art characterization tools and computational chemistry methods. In this work, thiol-treated palladium nanosheets are adopted as a model catalyst for the selective semihydrogenation of internal alkynes. Unexpectedly, thiol treatment created highly selective palladium catalysts with high activity toward the semihydrogenation reaction. The ultrathin nature of the as-prepared catalysts allows for the application of a variety of surface science and computational methods to resolve the complexity of metal-organic interfaces and thus elucidate the underlying mechanism. Driven by atomic-level understanding, we have realized practical, lead-free catalysts for semihydrogenation.

of Pd catalysts are usually passivated to prevent deep hydrogenation. With this strategy, Lindlar catalyst, a Pd/CaCO₃-based catalyst modified by a combination of both organic (quinoline) and inorganic (lead) additives, has been developed and widely used in industry for decades.³² Both the poor activity and the presence of toxic additives make the Lindlar catalyst not ideal for many industrial processes. Inspired by the Lindlar catalyst, increasing results have shown that surface modification of Pd or Pt catalysts can create a metal-organic interface that enhances their catalytic performance.³ The promotional effect of surface thiolates on the performance of Pd nanocatalysts has been reported repeatedly. For instance, Medlin and co-workers have demonstrated that the catalytic properties of Pd and Pt catalysts can be well controlled by coating *n*-alkane thiols on their surfaces.^{33–36} Although the importance of thiols or other sulfur-containing species in promoting palladium catalysis has been well understood in some Pd-complex systems,^{37–39} determination of the detailed surface and interface structure of thiolated-protected Pd nanocatalysts, and thus understanding the molecular mechanism behind the catalytic enhancements, remains challenging.

By using ultrathin Pd nanosheets (Pd NSs) as the metal substrate, we demonstrate here at the molecular level how thiols modify the surface of Pd nanocatalysts to dramatically enhance the selective hydrogenation of alkynes into alkenes. The ultrathin nature of Pd NSs makes it feasible to directly visualize the change in the surface structure of Pd NSs upon their reaction with thiols via electron microscopy. Our comprehensive characterizations reveal that upon adsorption, C–S bonds in thiols can be cleaved, forming a Pd surface modified with both thiolates and sulfides. Such a sulfide/thiolate modification creates both steric and electronic effects to prevent the hydrogenation of alkene intermediates during alkyne hydrogenation, endowing the modified Pd surface with high catalytic selectivity toward alkenes. With such an understanding, we have developed a facile strategy for preparing highly selective and stable Pd catalysts for semihydrogenation of internal alkynes by simply treating commercial Pd catalysts with thiols.

RESULTS

Synthesis and Structure Characterizations of Thiolate-Protected Pd Nanosheets

To create a model metal catalyst with metal-thiol interfaces that can be characterized in full, we chose ultrathin two-dimensional Pd NSs as the metal substrate for thiol surface modification in this work.⁴⁰ The ultrathin feature offers a high fraction of surface Pd atoms and thus allows the extraction of Pd-thiol interface structure information by spectroscopic techniques that normally collect both surface and bulk signals. In this study, uniform hexagonal Pd NSs (1.8-nm thick) with a diameter of 80 nm (Figure S1A) were prepared by a CO-assisted method. The Pd NSs were then mixed with 3,4-difluorothiols (HSPHF₂) in *N,N*-dimethylformamide (DMF) to induce thiol surface modification. The molar ratio of HSPHF₂/Pd was 1:1. The mixture was kept at 60°C for 12 hr before being cooled down to room temperature and centrifuged for collection of the product (see Supplemental Information). The as-modified Pd NSs were denoted as Pd@SPHF₂ (1:1). As revealed by transmission electron microscopy (TEM) (Figure 1A), the hexagonal shape of the original Pd NSs was heavily deformed after the thiol treatment.

The structure of the thiol-modified Pd NSs was characterized by various techniques. Lattice fringes of Pd 1/3(422) were clearly observed in the high-resolution TEM (HRTEM) image of Pd NSs (inset of Figure S1A), but it became impossible to

¹State Key Laboratory for Physical Chemistry of Solid Surfaces, Collaborative Innovation Center of Chemistry for Energy Materials, and Department of Chemistry, College of Chemistry and Chemical Engineering, Xiamen University, Xiamen 361005, China

²These authors contributed equally

³Lead Contact

*Correspondence: gfu@xmu.edu.cn (G.F.), nfzheng@xmu.edu.cn (N.Z.)

<https://doi.org/10.1016/j.chempr.2018.02.011>

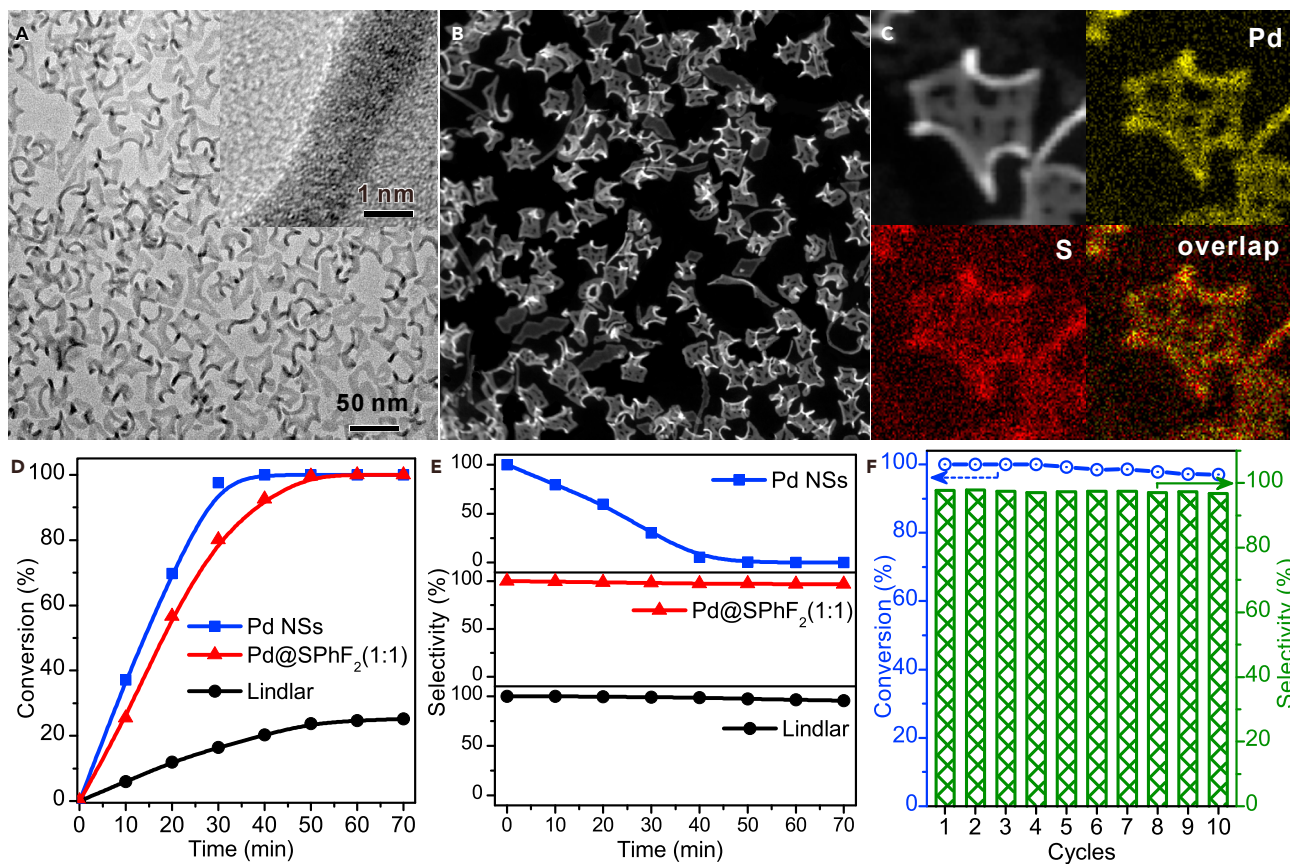


Figure 1. Structure Evolution of Pd NSs by Thiol Treatment and Their Catalytic Performance

(A–C) TEM and HRTEM images of Pd@SPhF₂(1:1) (A) and TEM and HRTEM images (B) and EDX mapping images (C) of an individual Pd@SPhF₂(1:1) nanoparticle.

(D) Catalytic performance of semihydrogenation of 1-phenyl-1-propyne with different Pd catalysts.

(E) Catalytic selectivity in semihydrogenation of 1-phenyl-1-propyne with different Pd catalysts.

(F) Catalytic stability and selectivity of the Pd@SPhF₂(1:1) obtained.

distinguish lattice fringes on Pd@SPhF₂ (1:1) from random noise because of their poor crystalline nature. After the reaction with thiol, the color of the Pd NSs solution changed from blue to dark gray with the disappearance of the broad peak at 1,100 nm in the ultraviolet-visible (UV-vis) spectrum (Figure S1B), demonstrating that their ultrathin metallic feature was altered. Moreover, as shown in the X-ray diffraction pattern of Pd@SPhF₂ (1:1), the Pd(111) peak at 40° was dramatically broadened, and the other diffraction peaks became negligible as a result of the formation of palladium sulfide on the surface of Pd NSs (Figures S1C and S1D). Simultaneously, the poor crystallinity of Pd@SPhF₂(1:1) was observed in the HRTEM analysis. High-angle annular dark field scanning transmission electron microscopy and energy-dispersive X-ray (EDX) elemental mapping (Figures 1B and 1C) revealed that both Pd and S were uniformly distributed throughout the Pd@SPhF₂ (1:1). All these results demonstrate that the thiol modification heavily modulated the surface structure of Pd NSs. Because of the ultrathin nature of Pd NSs, such a structure modulation readily induced an obvious morphological change that was detectable by TEM. It would be impossible to directly visualize the structure changes caused by surface ligand modification if Pd nanoparticles were used as the metal substrate.

High Catalytic Selectivity of Thiolate-Protected Pd Nanosheets in Hydrogenation of 1-Phenyl-1-propyne

The change in the structure and composition of Pd NSs is expected to influence their catalysis. Surprisingly, after the thiol treatment, Pd NSs readily served as a highly selective catalyst for the semihydrogenation of internal alkynyl compounds. When 1-phenyl-1-propyne was chosen as the model substance, as shown in Figures 1D and 1E, Pd@SPhF₂(1:1) exhibited an excellent selectivity of 98.1% toward 1-phenyl-1-propene at a conversion of 100% that was achieved within 50 min. In comparison, when the conversion of 1-phenyl-1-propyne reached 100%, the selectivity of the semihydrogenation product was only 30.5% over unmodified Pd NSs. In contrast, the Lindlar catalyst showed better selectivity than Pd NSs. But the main problem for the Lindlar catalyst is its low conversion rate. The conversion of 1-phenyl-1-propyne only reaches 25% within 70 min of the reaction. More impressively, no obvious decay in semihydrogenation selectivity was observed even after full conversion when Pd@SPhF₂(1:1) was used. The selectivity was maintained at ~97% in the ten cycles of catalysis in which very little decay in the activity was observed (Figure 1F). In comparison, Pd NSs maintained good activity in the five catalysis cycles, but displayed poor selectivity toward the semihydrogenation product (Figure S2A). When the Lindlar catalyst was used, an obvious decay in activity was observed although the selectivity was high (Figure S2B). Overall, Pd@SPhF₂(1:1) exhibited much better performance in the semihydrogenation of 1-phenyl-1-propyne than both unmodified Pd NSs and the Lindlar catalyst.

The enhanced catalytic selectivity motivated us to understand how the surface thiol modification modulates hydrogenation catalysis. The morphological transformation process of Pd NSs caused by surface thiol modification was first investigated by analysis of Pd NSs collected at different reaction times by TEM (Figures S3A–S3E). It was clearly revealed that the deformation process was initiated at the edges of the Pd NSs. Although only the edges became thicker at 0.5 hr, edge distortion was observed at 1.5 hr. The distortion process continued until 3 hr, beyond which no further morphological change was observed. Similarly, the optical absorption peak of the Pd NSs gradually decreased with the reaction time and disappeared after 3 hr (Figure S3F), consistent with the TEM observations. As revealed by the time-dependent EDX analysis (Figure S4), the sulfur content in the NSs increased with the reaction time and eventually reached ~25%. Moreover, the final morphology of Pd NSs depended on the SPhF₂/Pd ratio used in the modification process. As revealed by TEM and UV-vis analyses (Figure S5), whereas only edge deformation was observed with SPhF₂/Pd ratios of 0.2 and 0.5, extensive distortion took place with the SPhF₂/Pd ratio > 1. When the SPhF₂/Pd ratio increased from 0.2 to 0.5 to 1 to 5 to 10, the S/Pd ratio in the modified NSs increased by 12%, 21%, 26%, and 30%–32% (Figure S6). The sulfur content was not linearly increased with the SPhF₂/Pd ratio used in the modification. When the SPhF₂/Pd ratio was increased beyond 1, the content of S did not increase much. The catalytic performance of different ratios of SPhF₂/Pd is given in Figure S7. With an increased amount of thiol, the activity of the catalyst decreased and the selectivity increased. Interestingly, Pd@SPhF₂(1:1) exhibited both high reactivity and high selectivity.

Considering the large size of SPhF₂, its coverage on Pd cannot be high. The rather high S/Pd ratio on Pd@SPhF₂(1:1) suggested that S species should not be limited to SPhF₂ only. In order to study the nature of S, we extensively characterized the as-obtained Pd@SPhF₂ NSs by various means. Although the presence of SPhF₂ on Pd was confirmed by Fourier transform infrared spectroscopy (Figure S8), a temperature-programmed decomposition-mass spectrometry (TPD-MS) study illustrated

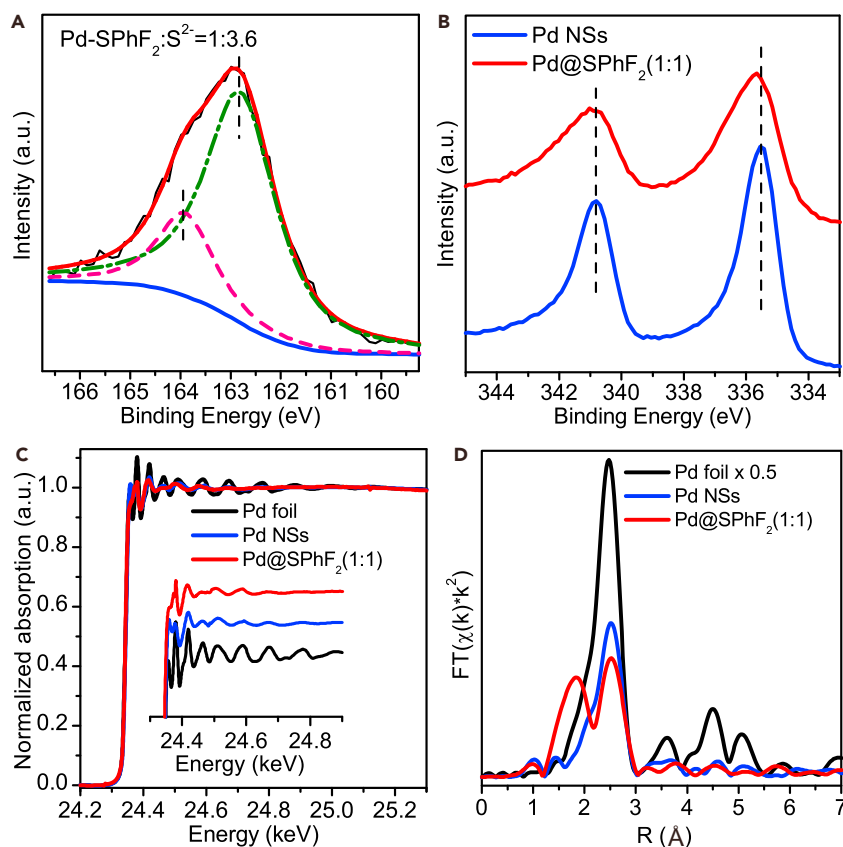


Figure 2. Structure Analysis of the Distorted Pd@SPhF₂ (1:1)

High-resolution XPS spectra of (A) the S 2p region and (B) the Pd 3d region and (C) Pd K-edge XANES and (D) FT-EXAFS spectra of the sample in comparison with untreated Pd nanosheets and Pd foil.

that SPhF₂ on Pd underwent S–C bond cleavage to release PhF₂ upon thermal treatment (Figure S9). Considering that temperature could have a great influence on S–C bond cleavage, the reaction was also conducted at room temperature for analysis of the temperature effect. Compared with the product obtained at 60°C, only the edge of Pd NSs was crimped at room temperature (Figure S10A). Moreover, when Na₂S was used to replace thiol, Pd NSs were heavily distorted as well (Figure S10B), indicating that S²⁻ generated by C–S cleavage should be responsible for the deformation of the Pd NSs. The low activity and high selectivity of Pd@Na₂S(1:1) (Figure S11) suggested that the sulfide-treated Pd NSs were overpassivated by S²⁻.

The X-ray photoelectron spectroscopic (XPS) data confirmed the co-presence of S²⁻ and thiolate on the thiol-treated Pd NSs. The overall S/Pd ratio of Pd@SPhF₂(1:1) was estimated to be 27%, consistent with the EDX result. In the XPS spectra of S 2p (Figure 2A), two main sulfur components at 162.9 and 163.8 eV were assigned to S²⁻ and SR⁻, respectively. The S²⁻/SR⁻ ratio was estimated to be 3.6. The presence of S²⁻ verified the S–C bond cleavage in the thiol modification process. Moreover, the binding energy of Pd 3d in distorted Pd NSs displayed a slight shift toward higher binding energy than that of unmodified NSs, indicating that Pd had been partial oxidized (Figure 2B). The peaks at 336.7 and 342.2 eV were assigned to Pd²⁺ 3d_{5/2} and Pd²⁺ 3d_{3/2}, respectively (Figure S12). Moreover, the XPS spectra of

different ratios of SPhF₂/Pd showed that, with the increased amount of SPhF₂, the ratio of S²⁻/SR⁻ was increased and eventually converged to about 1:5 (Figure S13). We proposed that the cleavage of C–S began at the edge and then the generated S²⁻ entered into the lattice of Pd NSs to form Pd_xS. With increasing HSPHF₂, Pd NSs were eventually fully converted into Pd_xS, whereas their surfaces were saturated by thiolate groups such that the ratio of SPhF₂/Pd reached a constant. To better understand the local environment of Pd, we further characterized the distorted Pd NSs by X-ray absorption fine structures (XAFS). Although Pd K-edge X-ray absorption near-edge structure spectrum (XANES) of Pd@SPhF₂(1:1) revealed the slightly oxidized nature of Pd (Figure 2C), the extended XAFS spectrum demonstrated that the coordination environment of Pd experienced a dramatic change upon thiol treatment (Figure 2D). Although the Pd–Pd coordination number was decreased from 9.7 to 4.7, a Pd–S scattering path appeared with the coordination number of 1.7. The Debye–Waller factor (σ^2) of Pd–Pd correlation increased from 6.2 to 12.3 after the thiol treatment, indicating the increase of local disorder in the Pd lattice (Figure S14 and Table S1). These data demonstrate that sulfur atoms entered the first coordination shell around Pd atoms after the thiol treatment, yielding Pd_xS species. To further characterize the 3D distribution of Pd and S elements, we used high-sensitivity low-energy ion scattering spectroscopy (Figure S15). Even with the increased depth detected, enabled by Ar ion sputtering, the presence of sulfur species was still revealed, indicating the incorporation of S²⁻ into the inner lattice of Pd.

Mechanism of the High Catalytic Selectivity by Thiolate-Protected Pd Nanosheets

To gain insight on how the thiol treatment enhanced hydrogenation selectivity, we performed periodic density functional theory (DFT) calculations (see Supplemental Information for computational details). The calculation results showed that cleavage of the C–S bond was able to take place on both Pd(111) and Pd(100) planes by overcoming a barrier of ~0.7 eV to deposit S²⁻ thereon (Figures S16 and S17). As previously reported, with increasing exposure to S-containing compounds, the as-generated atomic S would be incorporated into the subsurface region, yielding the palladium-sulfide interphase.^{41,42} Ni and co-workers also pointed out that the intermediate sulfide states, such as Pd₄S, Pd₃S, and Pd₁₆S₇, still have high catalytic activity toward the hydrogenation, whereas the catalyst would be deactivated completely when Pd was fully transformed into PdS.⁴³ Here, we used Pd₄S(110) and Pd₃S(100) coated with HSPHF₂ as models for Pd@SPhF₂(1:1) because they had the lowest surface energy among the low Miller index facets (Tables S3 and S4; Figures S18–S21). To be consistent with the experimental nomenclature, HSPHF₂-modified Pd₄S(110) and Pd₃S(100) surfaces are denoted as Pd₄S@SPhF₂ and Pd₃S@SPhF₂, respectively. These two models had similar composition and chemical environment to those of Pd@SPhF₂(1:1) (Table S5). We used both models to explore the observed high catalytic selectivity in the hydrogenation of internal alkynes (Figure 3A).

To understand why the catalytic selectivity of thiol-treated Pd NSs was better than the unmodified ones, we compared the hydrogenation of PhC≡CCH₃ over Pd₄S@SPhF₂, Pd₃S@SPhF₂ and bare Pd NSs. We assumed that all sides of the slabs were saturated with hydrogen under the hydrogenation conditions.⁴⁴ Catalytic hydrogenations generally follow the so-called Horiuti–Polanyi mechanism with a stepwise scheme involving the combination of co-adsorbed unsaturated hydrocarbon molecules and hydrogen atoms. On the basis of this mechanism, previous studies have proposed that a good catalyst for alkyne semihydrogenation should have a

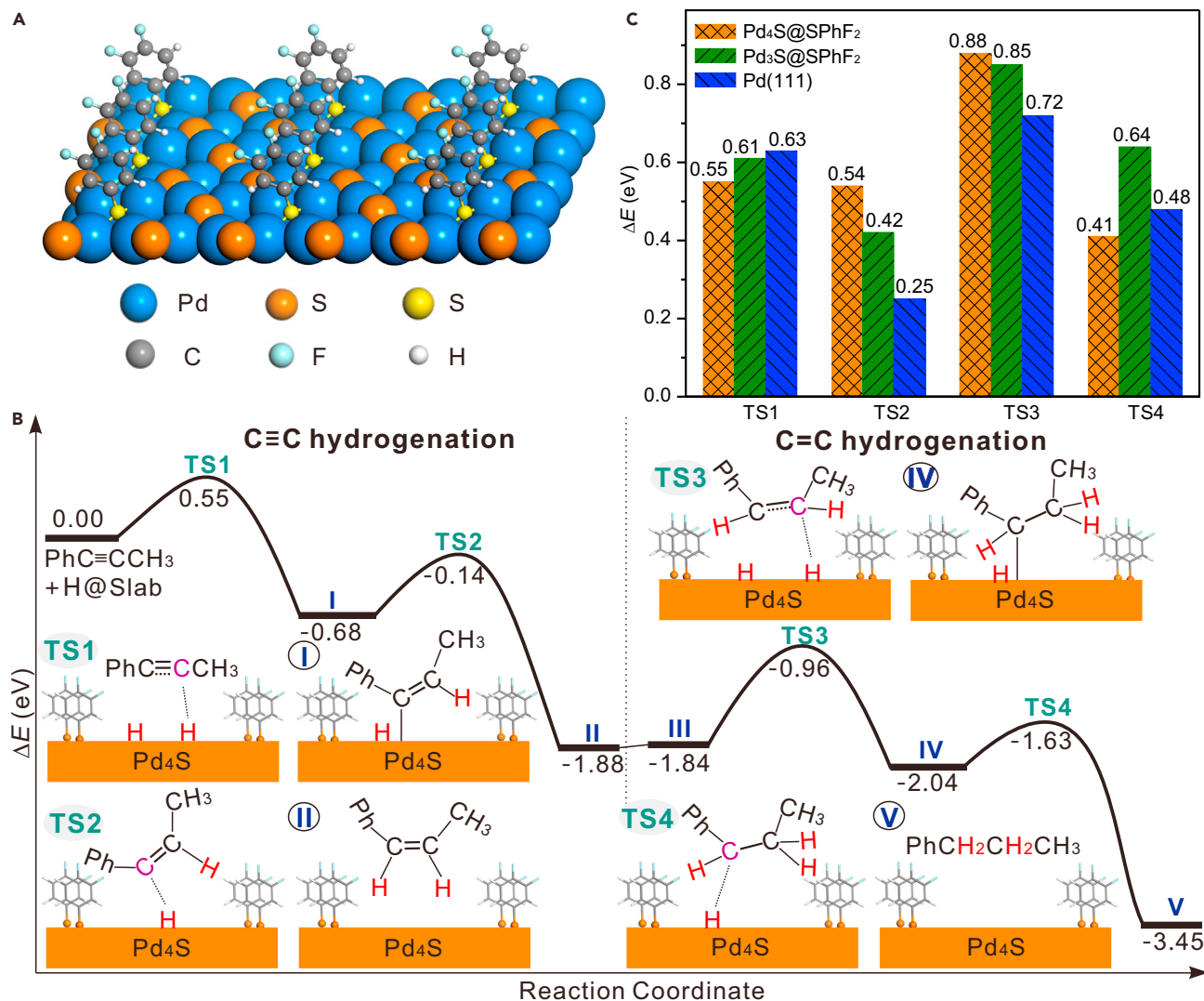


Figure 3. Mechanism of Catalytic Selectivity of Thiolate-Treated Pd NSs

(A) Constructed theoretical model of the Pd₄S@SPhF₂ surface.

(B) Energies of intermediates and transition states in the mechanism of PhC≡CCH₃ stepwise hydrogenation on the Pd₄S@SPhF₂ surface from DFT calculations.

(C) Energy barriers of transition states of PhC≡CCH₃ hydrogenation on Pd₄S@SPhF₂, Pd₃S@SPhF₂, and Pd(111).

higher barrier for the hydrogenation of alkene than its desorption barrier.^{44–46} However, in our case, neither PhC≡CCH₃ nor PhCH=CHCH₃ was able to adsorb on the hydrogen saturated surface so that hydrogenation could occur via an Eley-Rideal (ER) type mechanism.⁴⁷ Through the ER mechanism, unsaturated hydrocarbon molecules react with adsorbed hydrogen atoms directly. As illustrated in Figure 3B, the first hydrogenation step (C≡C to C=C) on Pd₄S@SPhF₂ involved two transition states (TS) (TS1 by the addition of the first hydrogen atom and TS2 by the addition of the second one) and a semihydrogenated intermediate (I) of C≡C hydrogenation. The second step (C=C to C–C) also proceeded through TS3 and TS4 by the addition of the third and fourth hydrogen atom, respectively, and one semihydrogenated intermediate (IV) of C=C hydrogenation. Obviously, a good semihydrogenation catalyst should promote the first hydrogenation step but inhibit the second one.

Figure 3C shows the calculated barriers for the four transition states during the hydrogenation of $\text{PhC}\equiv\text{CCH}_3$. The reaction energy profiles and the structures of key transition states and intermediates on $\text{Pd}_4\text{S@SPhF}_2$, $\text{Pd}_3\text{S@SPhF}_2$, and Pd(111) surfaces are shown in Figures S22–S26. It is clear that forming the semihydrogenated intermediate requires a higher barrier than its further hydrogenation. In other words, for the given catalyst, TS1 (or TS3) was higher than TS2 (or TS4). Thus, we used the difference in energy (ΔE_{TS}) between TS3 and TS1 to estimate the selectivity of semihydrogenation. DFT calculations demonstrated that ΔE_{TS} values for $\text{Pd}_4\text{S@SPhF}_2$ and $\text{Pd}_3\text{S@SPhF}_2$ were 0.33 and 0.24 eV, respectively, higher than that on bare Pd(111) surface (0.09 eV), nicely explaining why the selectivities of C=C on $\text{Pd}_4\text{S@SPhF}_2$ and $\text{Pd}_3\text{S@SPhF}_2$ were better than on Pd NSs. Through energy decomposition analysis (see details in Table S6), we found that such a significant difference in barrier mainly originated from $\Delta E_{\text{def}}(\text{S})$, the surface deformation energy. Close inspection on the transition-state structures revealed that thiolate groups had to deviate from the original structure to accommodate the alkene molecule (TS3), whereas the thiolate groups nearly maintained their structures when the alkyne molecule approached the surface (TS1). That is to say, it was the steric hindrance making the significant difference in ΔE_{TS} . Better adsorption of 1-phenyl-1-propyne on the H-free thiol-treated $\text{Pd@SPhF}_2(1:1)$ nanosheets than 1-phenyl-1-propene was observed experimentally (Figure S27).

Because the hydrogenation occurred via the ER mechanism, the reactivity critically depended on the adsorption energy of H. According to our calculations, the average adsorption energies of H on $\text{Pd}_4\text{S@SPhF}_2$ and $\text{Pd}_3\text{S@SPhF}_2$ were -0.05 and -0.03 eV, respectively, significantly weaker than that on Pd(111) (-0.52 eV). Nevertheless, H_2 dissociation was still feasible on the modified Pd surfaces. The calculated barriers for the cleavage of the H–H on $\text{Pd}_4\text{S@SPhF}_2$ and $\text{Pd}_3\text{S@SPhF}_2$ were predicted to be 0.55 and 0.33 eV, respectively (Figure S28). The weaker binding of H on thiol-treated Pd than on bare Pd can be attributed to the strong electronic effects induced by the presence of surface S^{2-} and thiolates. As determined by CO titration, the percentage of catalytic sites over the total Pd sites in $\text{Pd@SPhF}_2(1:1)$ was lower than that over Pd NSs (6% versus 20%). But compared with that of Pd NSs, the hydrogenation activity of $\text{Pd@SPhF}_2(1:1)$ in the selective hydrogenation of alkynes was not reduced much (Figure 1C). We consider the weaker adsorption of H as the main reason for the observed excellent hydrogenation activity of $\text{Pd@SPhF}_2(1:1)$ despite the presence of surface “poisoning” agents.

More interestingly, our DFT calculations also predicted that the major hydrogenation product of $\text{PhC}\equiv\text{CCH}_3$ should be *cis*- $\text{PhCH}=\text{CHCH}_3$. The rotation barrier of *cis*-SH11 was as high as 1.41 eV so that forming *trans*-I was kinetically inhibited (Figure S29). Impressively, the ^1H NMR data confirmed *cis*- $\text{PhCH}=\text{CHCH}_3$ as the major product when the thiol-treated Pd NSs were used as the catalyst (Figure S30). Moreover, DFT calculations also indicated that hydrogenation selectivity on $\text{Pd}_4\text{S@SPhF}_2$ surface should be quite different between internal and terminal alkynes. For instance, in the hydrogenation of $\text{PhC}\equiv\text{CH}$ on the $\text{Pd}_4\text{S@SPhF}_2$ surface, the predicted barrier for TS3 was only 0.65 eV (Figure S31), which was close to that of TS3 on an unmodified Pd(111) surface (0.61 eV) (Figure S32). This indicates that deep hydrogenation would take place when terminal alkynes are used as substrates. Experimentally, when phenylacetylene was used, the selectivity toward styrene was reduced to only 60.5% at 100% conversion of phenylacetylene (Figure S33), echoing the prediction from the DFT calculations.

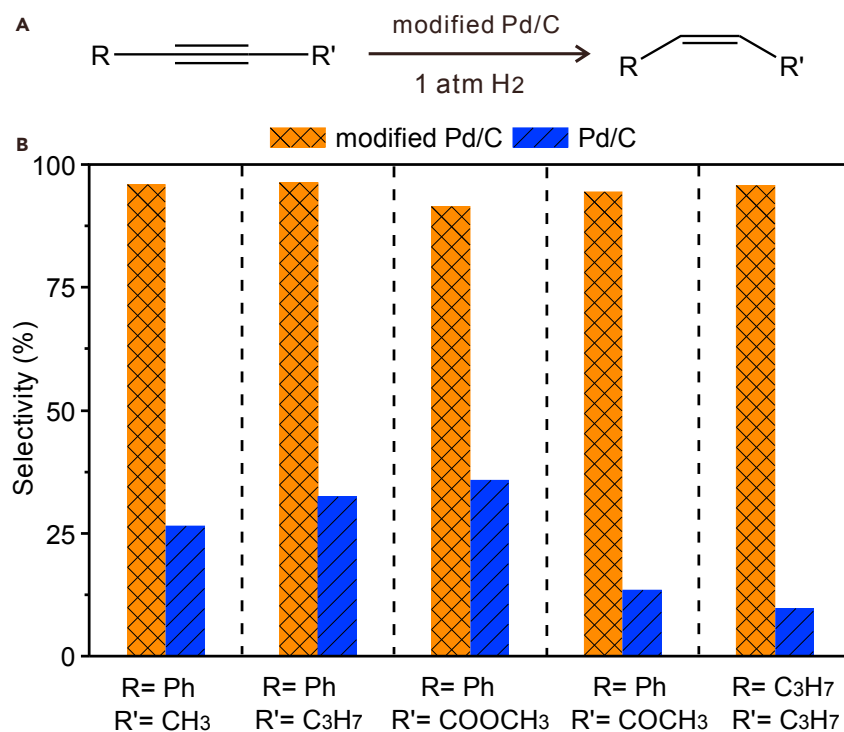


Figure 4. Optimization of Commercial Pd Catalysts via Thiol Treatment

(A) Schematic diagram of internal alkyne hydrogenation.

(B) Comparison of the catalytic performances for hydrogenation of substituted internal alkynes over commercial Pd/C before and after HSPHF₂ treatment.

DISCUSSION

The above studies demonstrate that the surface modification of both S²⁻ and RS⁻ on Pd resulted from the reaction between thiols and Pd NSs and was essential to the selective hydrogenation of alkynes to alkenes. We thus expected that treating conventional Pd nanoparticulate catalysts, such as Pd/C, with thiols should be an effective method of preparing highly selective catalysts for semihydrogenation of internal alkynes to alkenes. Experimentally, when Pd/C was treated with HSPHF₂ at 60°C, the modified catalyst turned out to be an efficient and selective catalyst for the semihydrogenation of 1-phenyl-1-propyne. In this case, there was no obvious change in the catalyst's morphology (Figure S34). The selectivity of the modified catalyst was also evaluated in the hydrogenation reactions of other internal alkynes (i.e., 1-phenyl-1-pentyne, methyl phenylpropiolate, 4-phenyl-3-butyne-2-one, 4-octyne). Compared with the unmodified Pd/C, the modified catalyst exhibited dramatically enhanced selectivity toward alkene products (Figure 4). Over the modified catalyst, the selectivity at 100% conversion was 96%, 92%, 94%, and 95% for 1-phenyl-1-pentyne, methyl phenylpropiolate, 4-phenyl-3-butyne-2-one, and 4-octyne, respectively (Figure S35). In comparison, the unmodified Pd/C gave poor selectivities of 32%, 10%, 36%, and 13%, respectively, under the same conditions (Figure S36).

These results further confirm the effectiveness of simple thiol treatment for promoting the catalytic selectivity of Pd nanocatalysts in the hydrogenation of internal alkynes to alkenes. Such an organic modification strategy is expected to not only provide a new research direction in engineering the surface of metal nanocatalysts

for fine chemical industries but also extend our understanding of the surface coordination chemistry of metal nanomaterials.⁴⁸

EXPERIMENTAL PROCEDURES

Synthesis of Pd Nanosheets

Pd(acac)₂ (50.0 mg), polyvinylpyrrolidone (160.0 mg), and tetra-*n*-butylammonium bromide (160 mg) were mixed together with DMF (10 mL) and water (2 mL) in a glass pressure vessel. The vessel was then charged with CO to 1 bar, heated from room temperature to 60°C in 0.5 hr, and then kept at 60°C for another 2.5 hr before it was cooled to room temperature. The dark blue products were precipitated by acetone, separated via centrifugation, and further purified by an ethanol-acetone mixture.

Synthesis of Different Ratios of Pd@SPhF₂ (1:0.2, 1:0.5, 1:1, 1:5, 1:10)

A Pd nanosheet stock solution (1 mL, 0.0137 mmol Pd) was precipitated by acetone and then dispersed in 5 mL of DMF in a glass vial. HSPHF₂ (0.3, 0.75, 1.5, 7.5, or 15 μL) was added into the mixture and then heated to 60°C for 12 hr. The products were collected by centrifugation with acetone. The products were dispersed in ethanol for further use.

Characterization

TEM studies were performed on a TECNAI F-30 high-resolution transmission electron microscope operating at 300 kV. The samples were prepared by dropping an ethanol dispersion of samples onto 300-mesh carbon-coated copper grids and immediately evaporating the solvent. All the UV-vis absorption spectra were taken on a Cary 5000 Scan UV-vis-near-infrared spectrophotometer (Varian) with ethanol as the solvent. Gas chromatography analyses were performed with a FuLi 9790II, equipped with a split/splitless injector, a capillary column (KB-5, 30 m × 0.32 mm × 0.33 μm), and a flame ionization detector.

X-Ray Absorption Spectroscopy Measurements

The X-ray absorption spectra at the Pd K-edge were recorded at room temperature in transmission mode with ion chambers at Beamline BL14W1 of the Shanghai Synchrotron Radiation Facility in China. The station was operated with a Si(311) double crystal monochromator. During the measurement, the synchrotron was operated at energy of 3.5 GeV and a current between 150 and 210 mA. The photon energy was calibrated with the first inflection point of Pd K-edge in Pd metal foil. The as-obtained X-ray absorption spectroscopy data were processed with WinXAS version 3.11. Reliable parameter values, such as bond distances, coordination numbers, etc., were determined via multiple-shell R-space fitting of Pd spectra.

TPD-MS Studies of Pd@SPhF₂

The TPD-MS experiment was performed on a home-made TPD-time-of-flight (TOF) analyzer. A 3 mg sample of Pd@SPhF₂(1:1) was pyrolyzed in a small tube heated by heating coil. A K-type thermocouple was put inside the sample tube and insulated from the samples for measuring the temperature. The heating coil was powered by a precise electric source and adjusted at intervals of 10 mV. The temperature of the sample tube was ramped from room temperature to 800°C smoothly at a speed of 5 K/min controlled by computer. The desorbed species were ionized by a UV lamp at a position very close to the sample tube with photon energy of 10.6 eV and then transferred to the TOF analyzer by an ion optical system. The TOF analyzer had a resolution of more than 5,000 and a sensitivity at ppb level. All these steps were processed in high vacuum at about 3 × 10⁻⁵ Pa. The mass

spectrum and sample temperature were acquired and recorded every second. Each spectrum is an accumulation of 10,000 spectra gathered at intervals of 100 s.

1-Phenyl-1-propyne Hydrogenation

The hydrogenation of 1-phenyl-1-propyne was carried out in a well-stirred glass pressure vessel (48 mL) at 30°C with stirring. A mixture of 0.05 mg of catalyst (Pd) and 1 mmol of substrate was dispersed in 10 mL of ethanol in the pressure vessel. H₂ flow was applied into the vessel for several minutes to remove oxygen. The vessel was then pressurized by 1.0 bar H₂. The reaction proceeded, and samples were withdrawn at regular intervals, filtered, and analyzed by gas chromatography. The product identity was further confirmed by gas chromatography-mass spectrometry.

SUPPLEMENTAL INFORMATION

Supplemental Information includes Supplemental Experimental Procedures, 36 figures, and 6 tables and can be found with this article online at <https://doi.org/10.1016/j.chempr.2018.02.011>.

ACKNOWLEDGMENTS

We acknowledge financial support from the Ministry of Science and Technology of China (2017YFA0207302 and 2015CB932303), the National Nature Science Foundation of China (21731005, 21420102001, 21390390, 21333008, 21373167, and 21573178), and the Fundamental Research Funds for the Central Universities (20720160046). We also thank the XAFS station (BL14W1) of the Shanghai Synchrotron Radiation Facility.

AUTHOR CONTRIBUTIONS

N.F.Z. conceived the idea. N.F.Z., X.J.Z., L.Y.Z., and G.F. co-wrote the paper. X.J.Z. synthesized the nanomaterials and carried out the catalysis experiments. G.F. and L.Y.Z. carried out the model construction and DFT calculations. W.Y.Z., C.Y.H., L.D., and L.T.R processed the relevant data. B.H.W. analyzed part of the data and polished the writing of the paper. All the authors contributed to the overall scientific interpretation and edited the manuscript.

DECLARATION OF INTERESTS

The authors declare no competing interests.

Received: September 19, 2017

Revised: November 7, 2017

Accepted: February 13, 2018

Published: March 22, 2018

REFERENCES AND NOTES

- Swiegers, G.F. (2008). Heterogeneous, Homogeneous, and Enzymatic Catalysis. A Shared Terminology and Conceptual Platform. The Alternative of Time-Dependence in Catalysis. In *Mechanical Catalysis: Methods of Enzymatic, Homogeneous, and Heterogeneous Catalysis*, G.F. Swiegers, ed. (John Wiley & Sons).
- Borodzinki, A. (2006). Selective hydrogenation of ethyne in ethene-rich streams on palladium catalysts. Part 1. Effect of changes to the catalyst during reaction. *Catal. Rev. Sci. Eng.* 48, 91–144.
- Vilé, G., Albani, D., Almora-Barrios, N., López, N., and Pérez-Ramírez, J. (2016). Advances in the design of nanostructured catalysts for selective hydrogenation. *ChemCatChem* 8, 21–33.
- Molnár, Á., Sárkány, A., and Varga, M. (2001). Hydrogenation of carbon-carbon multiple bonds: chemo-, regio- and stereo-selectivity. *J. Mol. Catal. Chem.* 173, 185–221.
- Zafeiratou, S., Piccinin, S., and Teschner, D. (2012). Alloys in catalysis: phase separation and surface segregation phenomena in response to the reactive environment. *Catal. Sci. Technol.* 2, 1787–1801.
- Sankar, M., Dimitratos, N., Miedziak, P.J., Wells, P.P., Kiely, C.J., and Hutchings, G.J. (2012). Designing bimetallic catalysts for a

- green and sustainable future. *Chem. Soc. Rev.* **41**, 8099–8139.
- Somorjai, G.A., and Rioux, R.M. (2005). High technology catalysts towards 100% selectivity: fabrication, characterization and reaction studies. *Catal. Today* **100**, 201–215.
 - Noyori, R. (2009). Synthesizing our future. *Nat. Chem.* **1**, 5–6.
 - Leeuwen, P.W.N.M.v. (2004). *Homogeneous Catalysis: Understanding the Art* (Kluwer Academic Publishers).
 - Bhaduri, S., and Mukesh, D. (2014). *Homogeneous catalysis: mechanisms and industrial applications*, second edition (John Wiley & Sons).
 - Schmid, A., Dordick, J.S., Hauer, B., Kiener, A., Wubbolts, M., and Witholt, B. (2001). Industrial biocatalysis today and tomorrow. *Nature* **409**, 258–268.
 - Wang, D.H., Engle, K.M., Shi, B.F., and Yu, J.Q. (2010). Ligand-enabled reactivity and selectivity in a synthetically versatile Aryl C–H olefination. *Science* **327**, 315–319.
 - Rod, T.H., and Nørskov, J.K. (2002). The surface science of enzymes. *Surf. Sci.* **500**, 678–698.
 - Bridier, B., López, N., and Pérez-Ramírez, J. (2010). Molecular understanding of alkyne hydrogenation for the design of selective catalysts. *Dalton Trans.* **39**, 8412–8419.
 - Segura, Y., Lopez, N., and Perez-Ramirez, J. (2007). Origin of the superior hydrogenation selectivity of gold nanoparticles in alkyne plus alkene mixtures: triple- versus double-bond activation. *J. Catal.* **247**, 383–386.
 - García-Mota, M., Bridier, B., Perez-Ramirez, J., and Lopez, N. (2010). Interplay between carbon monoxide, hydrides, and carbides in selective alkyne hydrogenation on palladium. *J. Catal.* **273**, 92–102.
 - García-Mota, M., Gomez-Diaz, J., Novell-Leruth, G., Vargas-Fuentes, C., Bellarosa, L., Bridier, B., Perez-Ramirez, J., and Lopez, N. (2011). A density functional theory study of the ‘mythic’ Lindlar hydrogenation catalyst. *Theor. Chem. Acc.* **128**, 663–673.
 - Chen, G., Xu, C., Huang, X., Ye, J., Gu, L., Li, G., Tang, Z., Wu, B., Yang, H., Zhao, Z., et al. (2016). Interfacial electronic effects control the reaction selectivity of platinum catalysts. *Nat. Mater.* **15**, 564–569.
 - Ye, R., Hurlburt, T.J., Sabyrov, K., Alayoglu, S., and Somorjai, G.A. (2016). Molecular catalysis science: perspective on unifying the fields of catalysis. *Proc. Natl. Acad. Sci. USA* **113**, 5159–5166.
 - Pachulski, A., Schoedel, R., and Claus, P. (2011). Performance and regeneration studies of Pd-Ag/Al₂O₃ catalysts for the selective hydrogenation of acetylene. *Appl. Catal. Gen.* **400**, 14–24.
 - Astruc, D., Lu, F., and Aranzas, J.R. (2005). Nanoparticles as recyclable catalysts: the frontier between homogeneous and heterogeneous catalysis. *Angew. Chem. Int. Ed.* **44**, 7852–7872.
 - Sa, J., Montero, J., Duncan, E., and Anderson, J.A. (2007). Bi modified Pd/SnO₂ catalysts for water denitration. *Appl. Catal. B Environ.* **73**, 98–105.
 - Semagina, N., and Kiwi-Minsker, L. (2009). Palladium nanohexagons and nanospheres in selective alkyne hydrogenation. *Catal. Lett.* **127**, 334–338.
 - Keresszegi, C., Grunwaldt, J.D., Mallat, T., and Baiker, A. (2003). Liquid phase oxidation of alcohols with oxygen: in situ monitoring of the oxidation state of Bi-promoted Pd/Al₂O₃. *Chem. Commun. (Camb.)*, 2304–2305.
 - Baber, A.E., Tierney, H.L., Lawton, T.J., and Sykes, E.C.H. (2011). An atomic-scale view of palladium alloys and their ability to dissociate molecular hydrogen. *ChemCatChem* **3**, 607–614.
 - Armbrüster, M., Kovnir, K., Behrens, M., Teschner, D., Grin, Y., and Schlögl, R. (2010). Pd-Ga intermetallic compounds as highly selective semihydrogenation catalysts. *J. Am. Chem. Soc.* **132**, 14745–14747.
 - Han, P., Axnanda, S., Lyubinsky, I., and Goodman, D.W. (2007). Atomic-scale assembly of a heterogeneous catalytic site. *J. Am. Chem. Soc.* **129**, 14355–14361.
 - Anderson, J.A., Mellor, J., and Wells, R.P.K. (2009). Pd catalysed hexyne hydrogenation modified by Bi and by Pb. *J. Catal.* **261**, 208–216.
 - Liu, M., Zhang, J., Liu, J., and Yu, W.W. (2011). Synthesis of PVP-stabilized Pt/Ru colloidal nanoparticles by ethanol reduction and their catalytic properties for selective hydrogenation of ortho-chloronitrobenzene. *J. Catal.* **278**, 1–7.
 - Mei, D., Neurock, M., and Smith, C.M. (2009). Hydrogenation of acetylene-ethylene mixtures over Pd and Pd-Ag alloys: first-principles-based kinetic Monte Carlo simulations. *J. Catal.* **268**, 181–195.
 - Tew, M.W., Emerich, H., and van Bokhoven, J.A. (2011). Formation and characterization of PdZn alloy: a very selective catalyst for alkyne semihydrogenation. *J. Phys. Chem. C* **115**, 8457–8465.
 - López, N., and Vargas-Fuentes, C. (2012). Promoters in the hydrogenation of alkynes in mixtures: insights from density functional theory. *Chem. Commun. (Camb.)* **48**, 1379–1391.
 - Schoenbaum, C.A., Schwartz, D.K., and Medlin, J.W. (2014). Controlling the surface environment of heterogeneous catalysts using self-assembled monolayers. *Acc. Chem. Res.* **47**, 1438–1445.
 - Kahsar, K.R., Schwartz, D.K., and Medlin, J.W. (2014). Control of metal catalyst selectivity through specific noncovalent molecular interactions. *J. Am. Chem. Soc.* **136**, 520–526.
 - Pang, S.H., Schoenbaum, C.A., Schwartz, D.K., and Medlin, J.W. (2013). Directing reaction pathways by catalyst active-site selection using self-assembled monolayers. *Nat. Commun.* **4**, 2448.
 - Marshall, S.T., O’Brien, M., Oetter, B., Corpuz, A., Richards, R.M., Schwartz, D.K., and Medlin, J.W. (2010). Controlled selectivity for palladium catalysts using self-assembled monolayers. *Nat. Mater.* **9**, 853–858.
 - Monfredini, A., Santacroce, V., Marchiò, L., Maggi, R., Bigi, F., Maestri, G., and Malacra, M. (2017). Semi-Reduction of internal alkynes with prototypical subnanometric metal surfaces: bridging homogeneous and heterogeneous catalysis with trinuclear all-metal aromatics. *ACS Sustain. Chem. Eng.* **5**, 8205–8212.
 - Ananikov, V.P., Orlov, N.V., Zaleskiy, S.S., Beletskaya, I.P., Khrustalev, V.N., Morokuma, K., and Musaev, D.G. (2012). Catalytic adaptive recognition of thiol (SH) and selenol (SeH) groups toward synthesis of functionalized vinyl monomers. *J. Am. Chem. Soc.* **134**, 6637–6649.
 - Drost, R.M., Rosar, V., Marta, S.D., Lutz, M., Demitri, N., Milani, B., de Bruin, B., and Elsevier, C.J. (2015). Pd-catalyzed Z-selective semihydrogenation of alkynes: determining the type of active species. *ChemCatChem* **7**, 2095–2107.
 - Huang, X., Tang, S., Mu, X., Dai, Y., Chen, G., Zhou, Z., Ruan, F., Yang, Z., and Zheng, N. (2011). Freestanding palladium nanosheets with plasmonic and catalytic properties. *Nat. Nanotechnol.* **6**, 28–32.
 - Radha, B., and Kulkarni, G.U. (2010). Patterned synthesis of Pd₂S: chemically robust electrodes and conducting etch masks. *Adv. Funct. Mater.* **20**, 879–884.
 - Love, J.C., Wolfe, D.B., Haasch, R., Chabynyc, M.L., Paul, K.E., Whitesides, G.M., and Nuzzo, R.G. (2003). Formation and structure of self-assembled monolayers of alkanethiolates on palladium. *J. Am. Chem. Soc.* **125**, 2597–2609.
 - Zhang, Q., Xu, W., Li, X., Jiang, D., Xiang, Y., Wang, J., Cen, J., Romano, S., and Ni, J. (2015). Catalytic hydrogenation of sulfur-containing nitrobenzene over Pd/C catalysts: in situ sulfidation of Pd/C for the preparation of Pd₂S₃ catalysts. *Appl. Catal. Gen.* **497**, 17–21.
 - Zhao, X., Zhao, Y., Fu, G., and Zheng, N. (2015). Origin of the facet dependence in the hydrogenation catalysis of olefins: experiment and theory. *Chem. Commun. (Camb.)* **51**, 12016–12019.
 - Li, J., Fleurat-Lessard, P., Zaera, F., and Delbecq, F. (2014). Mechanistic investigation of the cis/trans isomerization of 2-butene on Pt(111): DFT study of the influence of the hydrogen coverage. *J. Catal.* **311**, 190–198.
 - Studt, F., Abild-Pedersen, F., Bligaard, T., Sørensen, R.Z., Christensen, C.H., and Nørskov, J.K. (2008). Identification of non-precious metal alloy catalysts for selective hydrogenation of acetylene. *Science* **320**, 1320–1322.
 - Delbecq, F., Loffreda, D., and Sautet, P. (2010). Heterogeneous catalytic hydrogenation: is double bond/surface coordination necessary? *J. Phys. Chem. Lett.* **1**, 323–326.
 - Liu, P., Qin, R., Fu, G., and Zheng, N. (2017). Surface coordination chemistry of metal nanomaterials. *J. Am. Chem. Soc.* **139**, 2122–2131.